CORE
Metadata, citation and similar papers at core.ac.uk
Provided by UCL Discovery

The origin of second harmonic generation hotspots in chiral optical metamaterials [Invited]

V. K. Valev,[1,*] X. Zheng,[2] C.G. Biris,[3] A.V. Silhanek,[4] V. Volskiy,[2] B. De Clercq,[5] O. A. Aktsipetrov,[6] M. Ameloot,[5] N. C. Panoiu,[3] G. A. E. Vandenbosch,[2] and V. V. Moshchalkov[4]

[1]Molecular Electronics and Photonics, INPAC, Katholieke Universiteit Leuven, Leuven, Belgium
[2]ESAT-TELEMIC, K. U. Leuven, B-3001 Leuven, Belgium
[3]Department of Electronic and Electrical Engineering, University College London, Torrington Place, London WC1E 7JE, United Kingdom
[4]Superconductivity and Magnetism & Pulsed Fields Group, INPAC, Katholieke Universiteit Leuven, Leuven, Belgium
[5]University Hasselt and transnational University Limburg, BIOMED, Diepenbeek, Belgium
[6]Department of Physics, Moscow State University, 11992 Moscow, Russia
[7]Molecular Electronics and Photonics, INPAC, Katholieke Universiteit Leuven, Leuven, Belgium
**v.k.valev@fys.kuleuven.be*
www.valev.org

Abstract: Novel ways to detect the handedness in chiral optical metamaterials by means of the second harmonic generation (SHG) process have recently been proposed. However, the precise origin of the SHG emission has yet to be unambiguously established. In this paper, we present computational simulations of both the electric currents and the electromagnetic fields in chiral planar metamaterials, at the fundamental frequency (FF), and discuss the implications of our results on the characteristics of experimentally measured SHG. In particular, we show that the results of our numerical simulations are in good agreement with the experimental mapping of SHG sources. Thus, the SHG in these metamaterials can be attributed to a strong local enhancement of the electromagnetic fields at the FF, which depends on the particular structure of the patterned metamaterial.

© 2011 Optical Society of America

OCIS codes: (180.4315) Nonlinear microscopy; (240.4350) Nonlinear optics at surfaces; (160.1585) Chiral media; (160.3918) Metamaterials.

References and links

1. J. B. Pendry, A. J. Holden, D. J. Robbins, and W. J. Stewart, "Magnetism from conductors and enhanced nonlinear phenomen," IEEE Trans. Microw. Theory Tech. **47**(11), 2075–2084 (1999).
2. V. K. Valev, A. Kirilyuk, F. Dalla Longa, J. Kohlhepp, B. Koopmans, and Th. Rasing, "Observation of periodic oscillations in magnetization-induced second harmonic generation at the Mn/Co interface," Phys. Rev. B **75**(1), 012401 (2007).
3. H. W. K. Tom, T. F. Heinz, and Y. R. Shen, "Second-harmonic reflection from silicon surfaces and its relation to structural symmetry," Phys. Rev. Lett. **51**(21), 1983–1986 (1983).
4. O. A. Aktsipetrov, I. M. Baranova, E. D. Mishina, and A. V. Petukhov, "Lightning rod effect in surface-enhanced second-harmonic generation," JETP Lett. **40**, 1012–1015 (1984).
5. C. H. Lee, R. K. Chang, and N. Bloembergen, "Nonlinear electroreflectance in silicon and silver," Phys. Rev. Lett. **18**(5), 167–170 (1967).
6. A. Kirilyuk and Th. Rasing, "Magnetization-induced-second-harmonic generation from surfaces and interfaces," J. Opt. Soc. Am. B **22**(1), 148–167 (2005).
7. O. A. Aktsipetrov, T. V. Murzina, E. M. Kim, R. V. Kapra, A. A. Fedyanin, M. Inoue, A. F. Kravets, S. V. Kuznetsova, M. V. Ivanchenko, and V. G. Lifshits, "Magnetization-induced second- and third-harmonic generation in magnetic thin films and nanoparticles," J. Opt. Soc. Am. B **22**(1), 138–147 (2005).
8. Y. Sheng, A. Best, H.-J. Butt, W. Krolikowski, A. Arie, and K. Koynov, "Three-dimensional ferroelectric domain visualization by Cerenkov-type second harmonic generation," Opt. Express **18**(16), 16539–16545 (2010).
9. V. V. Pavlov, J. Ferré, P. Meyer, G. Tessier, P. Georges, A. Brun, P. Beauvillain, and V. Mathet, "Linear and non-linear magneto-optical studies of Pt/Co/Pt thin films," J. Phys. Condens. Matter **13**(44), 9867–9878 (2001).
10. J. D. Byers, H. I. Yee, and J. M. Hicks, "A second harmonic generation analog of optical rotatory dispersion for the study of chiral monolayers," J. Chem. Phys. **101**(7), 6233–6241 (1994).

#142180 - $15.00 USD Received 3 Feb 2011; revised 14 Mar 2011; accepted 14 Mar 2011; published 22 Apr 2011
(C) 2011 OSA

11. T. Petralli-Mallow, T. M. Wong, J. D. Byers, H. I. Yee, and J. M. Hicks, "Circular dichroism spectroscopy at interfaces: a surface second harmonic generation study," J. Phys. Chem. **97**(7), 1383–1388 (1993).
12. P. Fischer and F. Hache, "Nonlinear optical spectroscopy of chiral molecules," Chirality **17**(8), 421–437 (2005).
13. T. Verbiest, S. V. Elshocht, M. Kauranen, L. Hellemans, J. Snauwaert, C. Nuckolls, T. J. Katz, and A. Persoons, "Strong enhancement of nonlinear optical properties through supramolecular chirality," Science **282**(5390), 913–915 (1998).
14. S. Foerier, I. A. Kolmychek, O. A. Aktsipetrov, T. Verbiest, and V. K. Valev, "Optical second harmonic generation chiral spectroscopy," ChemPhysChem **10**(9-10), 1431–1434 (2009).
15. Y. Tang and A. E. Cohen, "Optical chirality and its interaction with matter," Phys. Rev. Lett. **104**(16), 163901 (2010).
16. C. Hubert, L. Billot, P.-M. Adam, R. Bachelot, P. Royer, J. Grand, D. Gindre, K. D. Dorkenoo, and A. Fort, "Role of surface plasmon in second harmonic generation from gold nanorods," Appl. Phys. Lett. **90**(18), 181105 (2007).
17. A. Lesuffleur, P. Gogol, P. Beauvillain, B. Guizal, D. Van Labeke, and P. Georges, "Nonlinear optical properties of interconnected gold nanoparticles on silicon," J. Appl. Phys. **104**(12), 124310 (2008).
18. A. Belardini, M. C. Larciprete, M. Centini, E. Fazio, C. Sibilia, M. Bertolotti, A. Toma, D. Chiappe, and F. Buatier de Mongeot, "Tailored second harmonic generation from self-organized metal nano-wires arrays," Opt. Express **17**(5), 3603–3609 (2009).
19. N. I. Zheludev and V. I. Emel'yanov, "Phase matched second harmonic generation from nanostructured metallic surfaces," J. Opt. A, Pure Appl. Opt. **6**(1), 26–28 (2004).
20. W. Fan, S. Zhang, N. C. Panoiu, A. Abdenour, S. Krishna, R. M. Osgood, K. J. Malloy, and S. R. J. Brueck, "Second harmonic generation from a nanopatterned isotropic nonlinear material," Nano Lett. **6**(5), 1027–1030 (2006).
21. J. Butet, J. Duboisset, G. Bachelier, I. Russier-Antoine, E. Benichou, C. Jonin, and P.-F. Brevet, "Optical second harmonic generation of single metallic nanoparticles embedded in a homogeneous medium," Nano Lett. **10**(5), 1717–1721 (2010).
22. J. Butet, G. Bachelier, J. Duboisset, F. Bertorelle, I. Russier-Antoine, C. Jonin, E. Benichou, and P.-F. Brevet, "Three-dimensional mapping of single gold nanoparticles embedded in a homogeneous transparent matrix using optical second-harmonic generation," Opt. Express **18**(21), 22314–22323 (2010).
23. C. Anceau, S. Brasselet, J. Zyss, and P. Gadenne, "Local second-harmonic generation enhancement on gold nanostructures probed by two-photon microscopy," Opt. Lett. **28**(9), 713–715 (2003).
24. N. J. Borys, M. J. Walter, and J. M. Lupton, "Intermittency in second-harmonic radiation from plasmonic hot spots on rough silver films," Phys. Rev. B **80**(16), 161407(R) (2009).
25. J. J. Maki, M. Kauranen, and A. Persoons, "Surface second-harmonic generation from chiral materials," Phys. Rev. B Condens. Matter **51**(3), 1425–1434 (1995).
26. S. Kujala, B. K. Canfield, M. Kauranen, Y. Svirko, and J. Turunen, "Multipole interference in the second-harmonic optical radiation from gold nanoparticles," Phys. Rev. Lett. **98**(16), 167403 (2007).
27. V. K. Valev, A. V. Silhanek, N. Verellen, W. Gillijns, P. Van Dorpe, O. A. Aktsipetrov, G. A. E. Vandenbosch, V. V. Moshchalkov, and T. Verbiest, "Asymmetric optical second-harmonic generation from chiral G-shaped gold nanostructures," Phys. Rev. Lett. **104**(12), 127401 (2010).
28. J. Butet, G. Bachelier, I. Russier-Antoine, C. Jonin, E. Benichou, and P.-F. Brevet, "Interference between selected dipoles and octupoles in the optical second-harmonic generation from spherical gold nanoparticles," Phys. Rev. Lett. **105**(7), 077401 (2010).
29. Y. Zeng, W. Hoyer, J. Liu, S. W. Koch, and J. V. Moloney, "Classical theory for second-harmonic generation from metallic nanoparticles," Phys. Rev. B **79**(23), 235109 (2009).
30. F. X. Wang, F. J. Rodríguez, W. M. Albers, R. Ahorinta, J. E. Sipe, and M. Kauranen, "Surface and bulk contributions to the second-order nonlinear optical response of a gold film," Phys. Rev. B **80**(23), 233402 (2009).
31. J. I. Dadap, J. Shan, K. B. Eisenthal, and T. F. Heinz, "Second-harmonic Rayleigh scattering from a sphere of centrosymmetric material," Phys. Rev. Lett. **83**(20), 4045–4048 (1999).
32. C. G. Biris and N. C. Panoiu, "Second harmonic generation in metamaterials based on homogeneous centrosymmetric nanowires," Phys. Rev. B **81**(19), 195102 (2010).
33. V. K. Valev, N. Smisdom, A. V. Silhanek, B. De Clercq, W. Gillijns, M. Ameloot, V. V. Moshchalkov, and T. Verbiest, "Plasmonic ratchet wheels: switching circular dichroism by arranging chiral nanostructures," Nano Lett. **9**(11), 3945–3948 (2009).
34. V. K. Valev, A. V. Silhanek, N. Smisdom, B. De Clercq, W. Gillijns, O. A. Aktsipetrov, M. Ameloot, V. V. Moshchalkov, and T. Verbiest, "Linearly polarized second harmonic generation microscopy reveals chirality," Opt. Express **18**(8), 8286–8293 (2010).
35. R. Dorn, S. Quabis, and G. Leuchs, "The focus of light-linear polarization breaks the rotational symmetry of the focal spot," J. Mod. Opt. **50**, 1917–1926 (2003).
36. Y. Schols and G. A. E. Vandenbosch, "Separation of horizontal and vertical dependencies in a surface/volume integral equation approach to model quasi 3-D structures in multilayered media," IEEE Trans. Antenn. Propag. **55**(4), 1086–1094 (2007).
37. M. Vrancken and G. A. E. Vandenbosch, "Hybrid dyadic-mixed potential integral equation analysis of 3D planar circuits and antennas," IEE Proc., Microw. Antennas Propag. **149**(5-6), 265–270 (2002).
38. M. O. D. Diffract, RSoft Design Group. http://www.rsoftdesign.com.
39. A. D. Rakic, A. B. Djurisic, J. M. Elazar, and M. L. Majewski, "Optical properties of metallic films for vertical-cavity optoelectronic devices," Appl. Opt. **37**(22), 5271–5283 (1998).

#142180 - $15.00 USD Received 3 Feb 2011; revised 14 Mar 2011; accepted 14 Mar 2011; published 22 Apr 2011
(C) 2011 OSA

40. T. F. Heinz, "Second-order nonlinear optical effects at surfaces and interfaces," in *Nonlinear Surface Electromagnetic Phenomena*, H. E. Ponath and G. I. Stegeman, eds. (Elsevier, 1991), pp. 353–416.
41. N. Bloembergen, R. K. Chang, S. Jha, and C. H. Lee, "Optical second-harmonic generation in reflection from media with inversion symmetry," Phys. Rev. **174**(3), 813–822 (1968).
42. C. K. Chen, A. R. B. de Castro, and Y. R. Shen, "Surface-enhanced second-harmonic generation," Phys. Rev. Lett. **46**(2), 145–148 (1981).
43. M. W. Klein, C. Enkrich, M. Wegener, and S. Linden, "Second-harmonic generation from magnetic metamaterials," Science **313**(5786), 502–504 (2006).
44. V. K. Valev, A. V. Silhanek, W. Gillijns, Y. Jeyaram, H. Paddubrouskaya, A. Volodin, C. G. Biris, N. C. Panoiu, B. De Clercq, M. Ameloot, O. A. Aktsipetrov, V. V. Moshchalkov, and T. Verbiest, "Plasmons reveal the direction of magnetization in nickel nanostructures," ACS Nano **5**(1), 91–96 (2011).

1. Both experimental and theoretical mapping of the SHG sources are required

Recently, Pendry and co-authors theoretically predicted that in specially engineered, metallic metamaterials, novel and enhanced nonlinear optical phenomena could be observed [1]. This idea stems from the fact that, in metallic metamaterials, there is a nonlinear dependence between the excitation field and the resulting local field enhancement. One major contribution to the local field enhancement is attributable to surface plasmon resonances. These are collective oscillations of the free electrons in metals, which can be readily excited by the electric field of light waves. Plasmon excitations with different physical properties can be generated upon nanopatterning a metal surface, namely: propagating (delocalized) plasmon waves or localized plasmon resonances. In other words, artificial surface structuring allows one to nano-engineer the local field intensity and spatial distribution that are due to plasmons. Consequently, plasmon-enhanced linear and nonlinear optical effects can be studiedachieved with nanopatterned metallic surfaces. Nonlinear optical effects, such as the second-, third-, or forth-harmonic generation, scale as the second, third or fourth power of the electromagnetic field intensity, respectively. Accordingly, nonlinear optical effects are very sensitive to electromagnetic field enhancements, such as those induced by plasmon excitation. It is expected, therefore, that nonlinear optical effects that are strongly dependent on the optical field inhomogeneity at nanoscale are achievable in metallic metamaterials.

Among the nonlinear optical effects observed upon light interaction with metallic structures, second harmonic generation (SHG) is particularly of interest because of its surface/interface symmetry sensitivity, down to the atomic level [2]. More generally speaking, this symmetry sensitivity is also present in higher-order harmonics, as long as they are even and the medium is centro-symmetric; this latter condition is satisfied by most metals with low optical losses. Besides its surface/interface sensitivity, SHG is especially sensitive to the symmetry properties of the crystalline lattice [3], to geometric features [4], as well as to externally applied electric [5] and magnetic [6,7] dc fields. More specifically, local or externally applied static electric and magnetic fields can break the symmetry of the material; consequently, SHG can be used effectively for imaging ferroelectric [8] and ferromagnetic [9] domains. In addition to rotation and time symmetry transformation, surface SHG is also sensitive to mirror symmetry transformations: chirality.

Historically, SHG studies of chiral symmetry breaking have been chiefly associated with chemistry, pharmacology, and biology. Specifically, many organic molecules are chiral and their handedness plays an important role in chemical reactions. It has been demonstrated that the SHG equivalents of optical rotatory dispersion (ORD) and circular dichroism (CD), designated as SHG-ORD [10] and SHG-CD [11], respectively, are typically several orders of magnitude more sensitive than their linear counterpart. Consequently, SHG techniques constitute particularly valuable spectroscopic tools for investigating the physical properties of thin layers, including molecular monolayers, fibers, surfaces, and membranes [12]. In such structures, supramolecular ordering can further increase the SHG signal; Fig. 1a illustrates this concept. The role of supramolecular ordering has been demonstrated in chiral helicene molecules [13], where the SHG-ORD and SHG-CD spectra yield very large signals [14]. Viewing chiral plasmonic resonators (meta-molecules) as the macroscopic counterpart of chiral molecules, it is expected that the SHG would be significantly enhanced upon

#142180 - $15.00 USD Received 3 Feb 2011; revised 14 Mar 2011; accepted 14 Mar 2011; published 22 Apr 2011
(C) 2011 OSA

distributing chiral plasmonic structures into a supramolecular chiral metasurface (see Fig. 1b) [15].

Plasmon-induced enhancement of SHG signal from a variety of nanosized objects, such as nanorods [16], chains of nanoparticles [17], nanowires [18] and periodically-structured arrays of nanostructures [19,20], has been recently reported. The SHG enhancement in a single gold metallic nanoparticle, 150 nm size, has also been observed [21,22]. Upon imaging, this local field enhancement appears as a hotspot. Such hotspots were also observed upon mapping the local enhancement of the SHG response from gold clusters consisting of 5 to 80 nanometer-sized metal grains, randomly distributed upon the surface of a silica substrate [23]. Similarly, SHG hotspots have been observed in rough silver films, where the hotspot was attributed to a single silver nanoparticle [24]. Nevertheless, while there is a well established theoretical framework for the SHG in regular materials [25], the origin and properties of SHG in plasmonic nanostructures poses a series of yet unanswered questions.

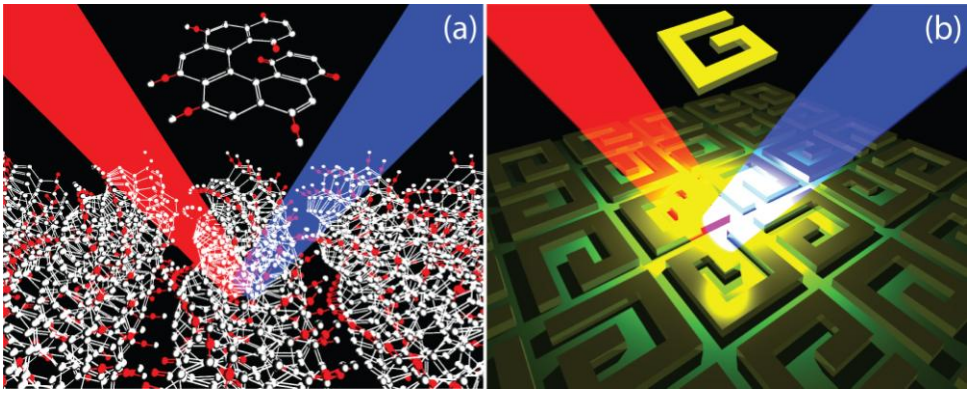

Fig. 1. Second harmonic generation methods for studying chirality were developed in organic molecules before being applied to metamaterials. In (a), illustration of SHG from supramolecularly ordered chiral helicenes molecules. In (b), illustration of SHG from G-shaped nanostructures, arranged in a chiral unit cell. The incoming light is at 800 nm (near red color) and the detected signal is at 400 nm (near blue color).

One of the main difficulties in characterizing the SHG from metallic nanoparticles stems from the fact that the SHG can be the result of several competing contributions, such as electric dipoles, magnetic dipoles and electric quadrupoles, and higher-order effects. In centrosymmetric materials, the (local) bulk electric dipole contribution to the SHG cancels and, therefore, the leading-order sources of the SHG are surface electric dipoles and the (nonlocal) contributions from bulk magnetic dipoles and electric quadrupoles. In metallic nanostructures, the local field enhancement and the corresponding large spatial variation of the field distribution increase the contribution to the SHG of both the surface and bulk components. Large multipolar contributions have thus been observed in plasmonic L-shaped [26] and G-shaped [27] metal nanostructures. Contributions from octupoles to the SHG signal of gold nanoparticles with size of ~100 nm have also been reported [28]. In this connection, a theoretical model that attributes most SHG to the bulk sources, thus explaining the enhancement of multipolar contribution to the SHG, has been proposed [29]. However, this same issue of surface versus bulk contribution to the SHG in nanostructured metal films has been investigated by Kauranen's group, the conclusion of this study being that the surface contribution dominates [30]. While the distribution of the local field enhancement at the fundamental frequency undoubtedly plays a role in the SHG response, both these studies lack an experimental mapping of the near-field distribution at the second harmonic.

To the best of our knowledge, the relationship between the local field enhancement at the fundamental frequency and the SHG in chiral metamaterials has not been unambiguously demonstrated yet. Because of the large dielectric constant of most metals, the near-field distribution in metallic nanostructures is extremely inhomogeneous. In previous theoretical

#142180 - $15.00 USD Received 3 Feb 2011; revised 14 Mar 2011; accepted 14 Mar 2011; published 22 Apr 2011
(C) 2011 OSA

studies the local field enhancement and spatial field inhomogeneity have been taken into account, for instance, when calculating the SHG response of spherical particles [31]. Generally, this procedure consists in three steps. First, the field at the fundamental frequency is determined numerically. Second, this fundamental frequency field is used to determine the nonlinear polarization (sources) at the second harmonic. And third, the electromagnetic field at the second harmonic is calculated (see, e.g [32].) by using the nonlinear polarization sources. Numerical simulations based on this approach can provide the spatial variation of the fundamental frequency and the second harmonic fields at the nanoscale although, in some cases, they can be time consuming and computationally demanding. To validate these numerical simulations, it is essential to develop alternative, experimental techniques, which then are to be used in conjunction with numerical methods to explore nonlinear optical effects at the nanoscale. To this end, we have recently demonstrated that SHG microscopy is a powerful tool for experimental mapping of the SHG sources in G-shaped nanostructures made of gold [27,33,34]. However, these experimental investigations were not yet validated by numerical simulations.

In this paper we present the results of a computational analysis of the spatial distribution of the local field enhancement at the fundamental frequency. In our study, we use MAGMAS' and RSoft's DiffractMOD software tools, which provide the surface currents and electromagnetic field distribution, respectively, generated upon the interaction between light and chiral metallic nanostructures. In both cases, the numerical maps of the local field enhancement at the fundamental frequency match the experimental mapping of SHG sources. Consequently, the origin of the SHG can unambiguously be attributed to maxima of the surface charge density, which in turn depend on the geometry of the structures. Our results suggest that SHG microscopy can be used efficiently for mapping the local field enhancement in nanostructured metamaterials.

2. We provide numerical simulations and experimental SHG microscopy

The sample preparation starts with a 200 mm single crystalline Si wafer, see Fig. 2a. On top of the wafer, a 100 nm thick layer of SiOx is thermally grown. The wafers are cleaned in two steps: first in a mixture of H_2SO_4/H_2O_2 and, second, in NH_4OH/H_2O_2/DIW mixture. Rinsing is performed in DIW. Next, a double resist layer of PMMA(polymethyl metacrylate)/co-PMMA, with thicknesses of 200 nm and 250 nm, respectively, is spun on top of the wafer, see Fig. 2b. On that double resist layer, high resolution electron beam lithography (EBL) is done with a VB6 system from Leica Microsystems Lithography, see Fig. 2c. The system is equipped with a thermal field emission electron source running at 20-100 kV providing a high brightness and small source size. Stage positioning is monitored by a laser interferometer with $\lambda/512 = 1.3$ nm precision. The VB6 system is also equipped with a real-time laser height sensor for dynamic field size corrections, and dynamic focus/astigmatism corrections all over the standard fields of 0.8192 mm (50 kV). The beam can be focused into a spot of 2 nm but proximity effects generated by unwanted secondary electrons and backscattered electrons raise this spot up to 25 nm. After the EBL exposure, the sample is immersed in a mixture of isopropyl alcohol and methyl isobutyl ketone for development, see Fig. 2d. Because of the lower molecular weight of co-PMMA with respect to PMMA, the bottom resist layer goes into solution faster than the top layer, making a convenient overhanging resist profile which facilitates the subsequent lift off procedure. Next, the remaining resist is subjected to a baking process, see Fig. 2e, which finalizes the preparation of the mask. The sample is now ready for material evaporation. Evaporation is done by sputtering of, first, a 3 nm thick Ti layer for adhesion, and then of 25 nm thick Au layer, see Fig. 2f. Once the metal layers are in place, it is time for the lift-off, i.e. the removal of the resist mask. To this purpose, the wafer is immersed in warm acetone or dichloromethane for a few minutes, see Fig. 2g, followed by an ultrasonic bath (few seconds). Then it is rinsed in iso-propanol and it is dried in a flow of nitrogen gas. The sample is then ready for SHG measurements, see Fig. 1h.

SHG microscopy images are collected with a confocal laser scanning microscope, Zeiss LSM 510 META (Jena, Germany). The sample is illuminated by a Mai-Tai DeepSee

#142180 - $15.00 USD Received 3 Feb 2011; revised 14 Mar 2011; accepted 14 Mar 2011; published 22 Apr 2011
(C) 2011 OSA

femtosecond pulsed Ti:Sapphire laser, directed to the sample by a dichroic mirror (HFT KP650) and through a Zeiss alpha PLAN-apochromat 100x/1.46 oil immersion objective. The fundamental excitation wavelength is 800 nm. The working distance of the 100x objective extends to 170 μm and the laser spot on the sample is elliptical, due to the high NA of 1.45 [35], with half axes 300 nm and 400 nm. After passing through a dichroic mirror (NFT545) and a short-pass filter (KP685), the SHG-signal is collected by photomultiplier tube. The image is formed with a scanning speed of 102.4 μs for the pixel dwell time; each line is scanned twice and averaged. Because optical sectioning is achieved through the multi-photon process, the confocal microscope pinhole diameter is set to its maximum value (open). The experimental data are then compared to numerical simulations.

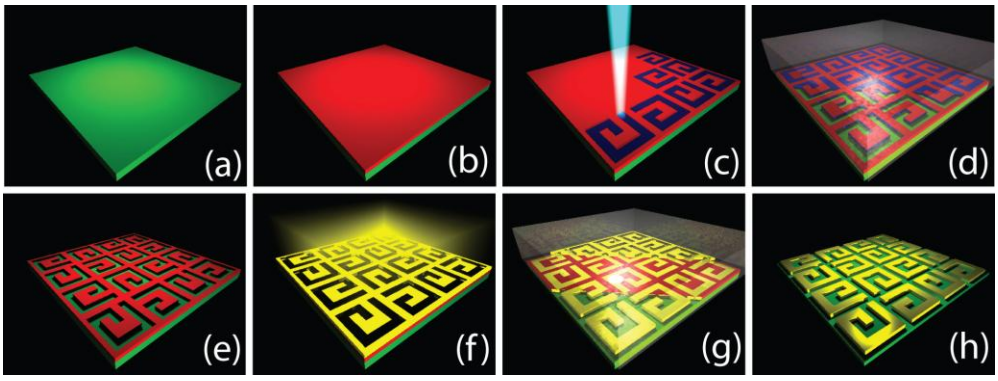

Fig. 2. Sample preparation. In (a), we start with a Si wafer. In (b), a double resist layer is spin-coated on the wafer. In (c), exposure: the nanostructures' pattern is drawn on the resist with electron beam lithography. In (d), development: a solvent removes the resist within the pattern. In (e), drying of the resist produces a mask. In (f), the mask is subjected to metal evaporation. In (g), lift-off: all the resist is removed in a solvent bath. In (h), the sample is ready.

MAGMAS is a numerical software tool, originally developed at the Katholieke Universiteit Leuven, for electromagnetic problems in the microwave and millimeter wave frequency bands [36,37]. It has been extended to include the special features of plasmonic nano-technology: (near) optical frequencies, strongly dispersive materials and the need for volumetric meshing. It formulates the Integral Equations for the structure under study, which are solved using the Method of Moments. MAGMAS is a so-called quasi-3D solver, which means that it is especially suited for topologies involving nano-components in multilayered structures. This is due to the fact that the multilayered background medium is taken into account analytically in the formulation. Only the actual components have to be meshed. Compared to differential equation techniques, like for example the finite-difference time-domain method, the resulting size of the numerical problem may be orders of magnitude smaller.

The field distribution at the fundamental frequency is calculated by using a commercially available software tool, RSoft's DiffractMOD [38]. The code implements a numerical method widely used in the analysis of optical properties of metallic and dielectric diffraction gratings, namely, the rigorous coupled-wave analysis method. Briefly described, the numerical method consists in decomposing in Fourier modes the reflected and transmitted fields, the corresponding modal amplitudes being determined by integrating across the structure a system of ordinary differential equations defined by the boundary conditions at the input and output facets of the periodic structure. The Fourier modes consist of both propagating and evanescent waves, which allows one to rigorously determine the spatial distribution of both the far- and near-field. In our simulations numerical convergence has been reached when 17 diffraction orders were used for each transverse dimension, which amounts to 35 Fourier modes. Moreover, we assumed that the dielectric constant of gold is described by the Lorentz-Drude model, with the interband effects being characterized by a superposition of four Lorentzians [39]. Our simulations have shown that the Ti adhesion layer does not affect the field

#142180 - $15.00 USD Received 3 Feb 2011; revised 14 Mar 2011; accepted 14 Mar 2011; published 22 Apr 2011
(C) 2011 OSA

distribution at the surface of the metallic structures although, as expected, it leads to larger overall absorption in the structure.

3. SHG depends on the local field enhancement at the fundamental frequency

The polarization at the second harmonic frequency can be written as [40]:

$$P_i(2\omega) \propto P_i^D(2\omega) + P_i^Q(2\omega) = \chi_{ijk}^{(2)} : \mathrm{E}_j(\omega)\mathrm{E}_k(\omega) + \chi_{ijkl}^{(3)} \vdots \mathrm{E}_j(\omega)\nabla_k \mathrm{E}_l(\omega), \quad (1)$$

where $\chi_{ijk}^{(2)}$ and $\chi_{ijkl}^{(3)}$ are second- and third-rank susceptibility tensors, respectively, while *i*, *j* and *k* represent any of the Cartesian coordinates *X*, *Y* and *Z*. The coordinate system is oriented so that *X*, and *Y* are in the plane of the sample, while *Z* is perpendicular to the sample. The first term in Eq. (1) is the *surface-specific* electric dipole contribution, indicated by the index *D*. The second term in Eq. (1) includes the *bulk-specific* electric quadrupole and magnetic dipole contributions, indicated by the index *Q*. In isotropic media, the latter take the following form [41]:

$$\begin{aligned}\mathbf{P}^Q(2\omega) = {} & (\chi_{XXXX} - \chi_{XYYX} - \chi_{XXYY} - \chi_{XYXY}) \sum_i \hat{e}_i E_i(\omega) \nabla_i E_i(\omega) \\ & + \frac{\chi_{XYXY}}{2} \nabla\left[\mathbf{E}(\omega)\cdot\mathbf{E}(\omega)\right] + \chi_{XYYX}\left[\mathbf{E}(\omega)\cdot\nabla\right]\mathbf{E}(\omega) + \chi_{XXYY}\mathbf{E}(\omega)\left[\nabla\cdot\mathbf{E}(\omega)\right].\end{aligned} \quad (2)$$

In metals, we can write [42]:

$$\mathbf{P}^Q(2\omega) \propto \chi_{XYYX}\left[\mathbf{E}(\omega)\cdot\nabla\right]\mathbf{E}(\omega) + \chi_{XXYY}\mathbf{E}(\omega)\left[\nabla\cdot\mathbf{E}(\omega)\right]. \quad (3)$$

If we assume that $\mathbf{E}_{local}(\omega) = L(\omega)\mathbf{E}(\omega)$, where $L(\omega)$ represents the local field factors for the fundamental frequency [41], it then follows that, for the dipolar contributions:

$$\begin{aligned}P_{i,local}^D(2\omega) &\propto L(2\omega)\chi_{ijk}^{(2)} : \mathrm{E}_{j,local}(\omega)\mathrm{E}_{k,local}(\omega) \\ &\propto L(2\omega)L^2(\omega)P_i^D(2\omega),\end{aligned} \quad (4)$$

where $L(2\omega)$ represents the local field factors at the second harmonic frequency. The local field factors $L(\omega)$ and $L(2\omega)$ contain the contributions from plasmonic excitations, such as those observed in our nanostructures. Furthermore, for the quadrupolar contributions:

$$\begin{aligned}\mathbf{P}_{local}^Q(2\omega) \propto {} & L(2\omega)\chi_{XYYX}\left[L(\omega)\mathbf{E}(\omega)\cdot\nabla\right]L(\omega)\mathbf{E}(\omega) \\ & + L(2\omega)\chi_{XXYY}L(\omega)\mathbf{E}(\omega)\left[\nabla\cdot L(\omega)\mathbf{E}(\omega)\right].\end{aligned} \quad (5)$$

Combining Eqs. (4) and (5), we obtain:

$$\mathbf{P}_{local}(2\omega) = L(2\omega)L^2(\omega)\mathbf{P}(2\omega). \quad (6)$$

And henceforth, the intensity at the second harmonic can be expressed as:

$$I(2\omega) \propto \left|L(2\omega)L^2(\omega)\mathbf{P}(2\omega)\right|^2. \quad (7)$$

This relationship implies that, in metal nanostructures, we expect a correspondence between the distribution of local field enhancements at the fundamental frequency and the SHG sources.

4. SHG matches the numerical simulations performed at the fundamental frequency

In Fig. 3a and Fig. 3b, the geometry of the G-shaped and mirror-G-shaped nanostrucres, respectively, can be seen. For these structures, under the influence of linearly polarized light,

#142180 - $15.00 USD Received 3 Feb 2011; revised 14 Mar 2011; accepted 14 Mar 2011; published 22 Apr 2011
(C) 2011 OSA

SHG microscopy reveals four hotspots that are positioned along the diagonals in Fig. 3c and Fig. 3d. This result has already been reported, though the precise location of the hotspot on the structures was not clear [33,35].

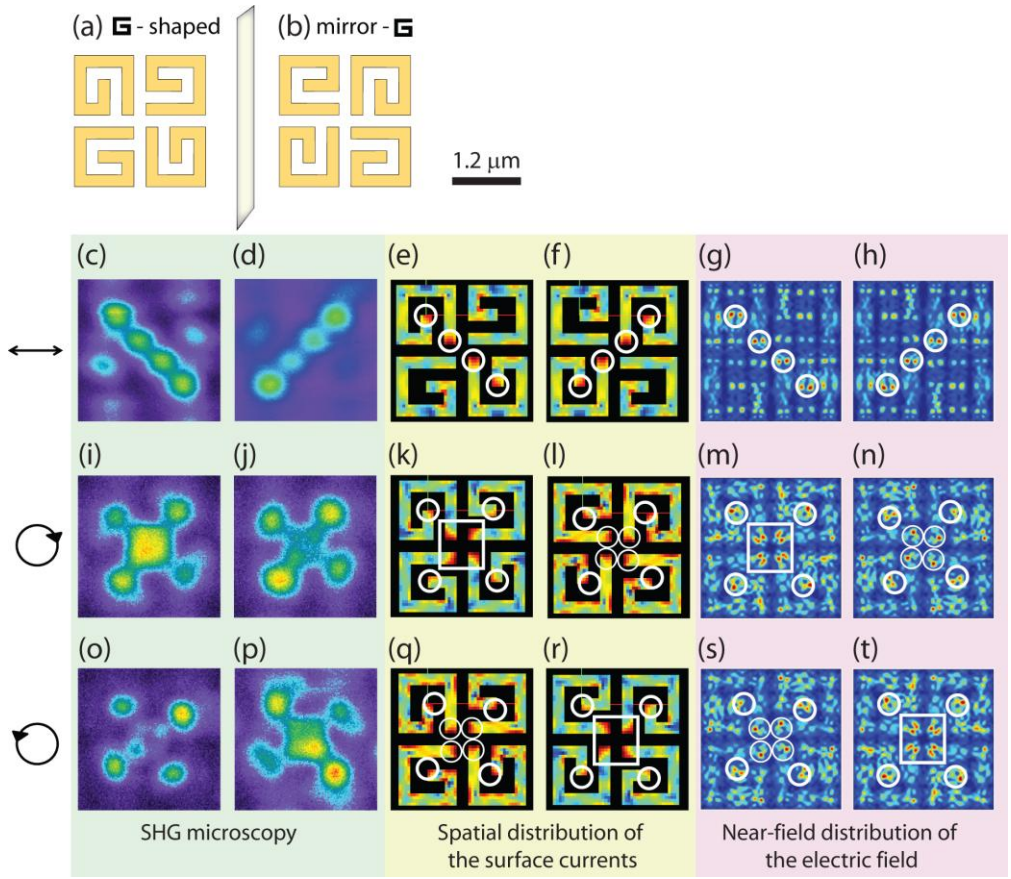

Fig. 3. Mapping of the SHG sources matches the mapping of surface field enhancements at the fundamental frequency. In (a) and (b), the geometry of the two sample configurations that were used for the gold nanostructures. Experiments and calculations were performed for linearly, right-hand and left-hand circularly polarized light as indicated on the left side. The images are organized columnwise according to the sample. The images (c), (i), (o), (e), (k), (q), (g), (m), (s) and (d), (j), (p), (f), (l), (r), (h), (n), (t) refer to G-shaped and mirror-G, respectively. The first two columns of the images are obtained with SHG microscopy. The third and fourth columns are calculated with the MAGMAS software. The fifth and sixth columns are obtained with the DiffractMOD software.

In order to clarify the location of the hotspots, numerical simulations of the electrical currents at the fundamental frequency were performed with the MAGMAS software. Note that this software calculates the surface currents, which are expected to be proportional with the local field enhancement. Figure 3e and Fig. 3f show the resulting maps of local field enhancements at the surface of the nanostructures. In each case, the strongest field enhancements are situated in four regions that correspond to the SHG hotspots. Because these simulations do not take into account the dielectric, the substrate, and the Ti adhesion layer, their agreement with the SHG results demonstrates that the electromagnetic behavior of the gold nanostructures is the main cause for the SHG signal. Moreover, numerical simulations of the electric fields at the fundamental frequency were performed with the DiffractMOD software. Neither these simulations nor those performed with MAGMAS took into account the substrate. Nevertheless, the results in Fig. 3g and Fig. 3h are in remarkable agreement with both MAGMAS simulations and the SHG microscopy. For better comparison with the SHG,

#142180 - $15.00 USD Received 3 Feb 2011; revised 14 Mar 2011; accepted 14 Mar 2011; published 22 Apr 2011
(C) 2011 OSA

the DiffractMOD results show the squared electric fields at the surface of the nanostructures. The agreement between the experimental results at the second harmonic and both simulations at the fundamental frequency can also be observed for right-hand circularly polarized light, Fig. 3i to Fig. 3n, as well as for left-hand circularly polarized light, Fig. 3o to Fig. 3t. It should be noted that for circularly polarized light, there is a large circular dichroism effect both in the SHG and in the simulations. In fact, regarding SHG this effect has previously been reported, though, as with linearly polarized light, the location and origin of the hotspot patterns was ambiguous. It should be noted that both the MAGMAS and the DiffractMOD simulations were performed with a linearly polarized light and did not take into account the tight focusing of the beam; the incident beam was assumed to be a plane wave. The agreement between simulations and experimental results clearly shows that the tight focusing does not constitute a crucial factor, which is explained by the fact that the hotspot formation is chiefly a near-field effect.

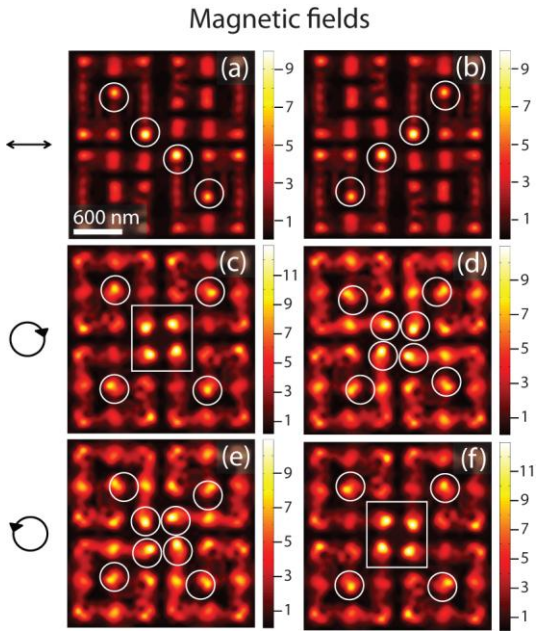

Fig. 4. Magnetic fields at the surface of the gold nanostructures also match the distribution of SHG sources. In (a), (c) and (e), magnetic field intensity in G-shaped nanostructures, for linearly, right-hand circularly and left-hand circularly polarized light, respectively. In (b), (d) and (f), magnetic field intensity in mirror-G-shaped nanostructures, for linearly, right-hand circularly and left-hand circularly polarized light, respectively. The white lines are guides to the eye, highlighting the correspondence to the SHG microscopy patterns.

The simulations results in Fig. 3, pinpoint the exact location of the hotspots on the structures and establish a clear relationship between the location of the second harmonic sources and local field enhancements of the *electrical* currents and field, at the fundamental frequency. But what about the *magnetic* field?

In optical metamaterials, it was suggested that larger SHG signals could be detected when magnetic-dipole resonances are excited, as compared with purely electric-dipole resonances [43]. In order to investigate the magnetic fields at the fundamental optical frequency in our structures, DiffractMOD simulations were performed and the resulting maps are shown in Fig. 4. Starting with the G-shaped nanostructures, as it can be seen for linearly, right-hand circularly and left-hand circularly polarized light in Fig. 4a, Fig. 4b, and Fig. 4c, respectively, the maxima of the magnetic field intensities correspond to the SHG microscopy patterns, indicated with white lines. This same correspondence is also observed with the mirror-G-shaped nanostructures, in Fig. 4d, Fig. 4e, and Fig. 4f.

#142180 - $15.00 USD Received 3 Feb 2011; revised 14 Mar 2011; accepted 14 Mar 2011; published 22 Apr 2011
(C) 2011 OSA

According to Eq. (7), the local field effects take the form of a multiplication factor to both the surface (electric dipoles) and the bulk (magnetic dipoles, electric quadrupoles, etc.) contributions to the SHG intensity. The expected correspondence between the patterns of SHG sources and the patterns of local field enhancements at the fundamental frequency was experimentally verified, as shown in Fig. 3 and Fig. 4. Our results demonstrate that the origin of SHG in these structures is determined by the local field enhancements at the fundamental frequency.

5. SHG microscopy is an efficient technique for mapping local field enhancements

In conclusion, while previous studies of the origin of SHG in metamaterials accurately predicted the overall SHG intensity for different polarized-analyzer configurations and dependence on quarter-wave plate rotation, they did not map the actual SHG sources on the nanostructures. In this paper we demonstrated that experimental mapping of the SHG sources matches very well with the results of numerical simulations of the local field enhancements at the fundamental frequency. Our results are in perfect agreement with the existing theoretical framework for SHG enhancements from local field factors. The numerical simulations presented here could be extended to the second harmonic response in order to reproduce the overall SHG intensity for different polarized-analyzer configurations and quarter- or half-wave plate rotation dependences.

From a practical point of view, our data demonstrate that SHG microscopy constitutes an imaging method for mapping local field enhancements in metamaterials. This new visualization tool is important because it has been instrumental in exploring the novel properties of chiral optical metamaterials. Also, SHG imaging is a very helpful technique as the images that were revealed from the nanostructures are surprising and counter-intuitive. Furthermore, our application of SHG is user friendly due to the fact that a commercial confocal microscope was adapted for SHG imaging and the samples followed a standard preparation procedure. Moreover, SHG imaging appears to be widely applicable since successful imaging was obtained from different shapes (Gs, Us, Ls and Is) and different materials, such as Au [33], Ni [44] and, most recently, Pd.

Acknowledgments

We acknowledge financial support from the Fund for scientific research Flanders (FWO-V), the University of Leuven (GOA), Methusalem Funding by the Flemish government and the Belgian Inter-University Attraction Poles IAP Programmes. V.K.V., and A.V.S. are grateful for the support from the FWO-Vlaanderen. C.G.B. and N.C.P. acknowledge support from the UK Engineering and Physical Sciences Research Council (EPSRC). O.A.A. is partly supported by the Russian Foundation for Basic Research (RFBR). B. DeC. is grateful to the IWT.

#142180 - $15.00 USD Received 3 Feb 2011; revised 14 Mar 2011; accepted 14 Mar 2011; published 22 Apr 2011
(C) 2011 OSA